UNIVERSITY OF BIRMINGHAM

University of Birmingham Research at Birmingham

Mean pressure distributions and reattachment lengths for roof-separation bubbles on low-rise buildings

Akon, A.F.; Kopp, Gregory

Link to publication on Research at Birmingham portal

Mean Pressure Distributions and Reattachment Lengths for Roof-Separation Bubbles on Low-Rise Buildings

Abul Fahad Akon, Gregory A. Kopp

Boundary Layer Wind Tunnel Laboratory, Faculty of Engineering, University of Western Ontario, London, ON, Canada N6A 5B9.

Abstract

Investigations of separated and reattaching flows near the leading edge of three-dimensional bluff bodies placed in turbulent boundary layers are important because of the large aerodynamic loads that these flows cause. Roofs of low-rise buildings are vulnerable to this kind of wind loading. Turbulence properties in the approaching boundary layer flow affect the pressure distributions and the mean size of the separation bubble formed on building surfaces. In this study, the effects of turbulence intensities and length scales in the incident boundary layer on the mean reattachment lengths and surface mean pressure distributions for low-rise building roofs are investigated. Particle Image Velocimetry measurements of the roof separation bubble, along with surface measurements, for a low-rise building model were taken for six different, upstream, boundary-layer conditions. Surface pressure measurements were taken for a second building model in similar upstream conditions. Along with these data, pressure data from the NIST aerodynamic database were used in the analysis. The mean size of the roof separation bubble is found to be unaffected by the turbulence length scales over the range tested, whereas turbulence intensity has a significant effect on reattachment lengths. The mean pressure distribution was found to be a function of both the mean reattachment length and the upstream turbulence intensity. A method of estimating the mean reattachment length on the roof of low-rise buildings from measured surface pressures and roof height turbulence intensity is proposed.

Keywords

Building aerodynamics; atmospheric boundary layers; low-rise buildings; turbulence; separated flows; reattaching flows.

1. Introduction

Separating and reattaching flows on the surface of sharp-edged, elongated bluff bodies are of fundamental importance to the aerodynamic loads for these shapes. The flow near the leading edge of such bodies has received special attention by researchers since there are large pressure fluctuations on the surface beneath the separating – reattaching flow (Lyn & Rodi, 1994; Saathoff & Melbourne, 1997). These cause large uplifting loads (e.g., on the roofs of low-rise buildings (Tieleman *et al.*, 1996) or can interact with the trailing edge, leading to the flow instabilities such as vortex streets in the wake (e.g., on long-span bridges, Taylor *et al.*, 2014). In the present paper, the focus is on the mean pressure field beneath separation bubbles on surface-mounted prisms in turbulent boundary layers. Figure 1 shows a schematic representation of the terminologies used to describe separating-reattaching flows over sharp-edged, elongated, bluff bodies. In particular, the point on the bluff-body surface where the mean flow reattaches is known as the reattachment point, the distance between the separation point and the reattachment point is defined as the reattachment length.
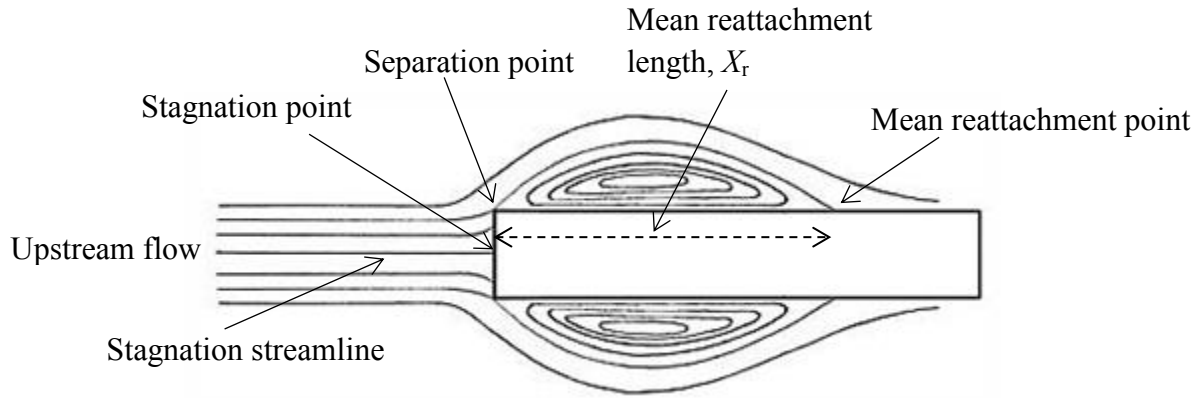
Figure 1: Schematic diagram of a separating and reattaching flow over a sharp-edged, elongated, two-dimensional bluff body placed in uniform upstream flow.

1.1 Two-dimensional Bluff Bodies

Ruderich and Fernholz (1986) investigated the nature of the mean pressure field beneath separating – reattaching flows and found similarity of the distribution when the mean pressure coefficients are normalized by the minimum pressure such that the reduced pressure coefficient is:

$$C_p^* = \frac{(C_p - C_{p,\min})}{1 - C_{p,\min}} \tag{1}$$

where C_p is the mean pressure coefficient, $C_{p,\min}$ is the minimum value of the mean pressure coefficient on the surface under the separation bubble, while streamwise distance, x, is normalized by the reattachment length, X_r. Eq. 1 was first proposed by Roshko & Lau (1965). The experimental results of Hudy *et al.* (2003) were found to be similar to the results of Ruderich and Fernholz (1986). These authors found that, for a smooth (i.e., low turbulence) free stream, irrespective of Reynolds numbers, body shape, blockage ratio, over a large range of reattachment lengths, the distribution of

reduced pressure coefficients fall on the same curve. However, the reasons for the particular shape of the curve, or how surface pressures arise, were not explained.

Researchers have shown that the flow structure of separation bubbles, the surface pressure and aerodynamic forces on the body beneath the separation bubble, and the reattachment length are strongly dependent on the turbulence parameters in the upstream flow (e.g., Gartshore, 1973; Hillier & Cherry, 1981). Upstream properties affecting the separation bubble properties are turbulence intensities, $I_u = \frac{\sigma}{U}$ (where, σ is the standard deviation of the velocity fluctuations and U is the streamwise mean velocity), and the turbulent scales, particularly the integral scales, $L = \int_0^\infty r(\xi)\, d\xi$, relative to the dimensions of the body, where $r(\xi)$ is the correlation coefficient of the velocities separated by some distance, ξ. Usually the integral scale, L_x, formed by the streamwise velocities separated in the streamwise direction, x, is considered to be the most important integral scale.

Hot-wire measurements in the separation bubble by Hillier & Cherry (1981) for different turbulence intensities and integral length scales show that higher levels of the free-stream turbulence intensity causes a reduction in the reattachment length, but that the reattachment length tends to be insensitive to the integral scales. Kiya & Sasaki (1983) and Saathoff & Melbourne (1997) also found similar trends in the reduction of the reattachment length with turbulence intensity. These authors suspected that the higher levels of entrainment in the turbulent flow cases are responsible for the smaller reattachment lengths. These studies were performed on two-dimensional bluff bodies of thickness, D, in uniform flow over a range of turbulence intensities up to 15% and length scales, L_x/D, up to 2.1. However, the effects of length scales on mean reattachment lengths for larger ranges of turbulence length scales have not yet been investigated. Nakamura & Ozono (1987) investigated the surface mean pressures under the separated and reattaching flows for an extended range of integral length scales ($L_x/D = 0.4$ to 24), focussing on the maximum turbulence-intensity levels investigated by Hillier & Cherry (1981) and Kiya & Sasaki (1983). Their investigation indicated an independence of the surface mean pressure distribution at smaller ratios of integral scale to body thickness. However, for higher ratios of integral scales to body thickness, they observed dependence of the mean surface pressures to the integral scales. These results indicate that larger integral scales may have some effect on the mean reattachment length.

Perhaps the most investigated property of separation bubbles is the surface pressure field because of the practical importance. The properties of free-stream turbulence are known to significantly affect the mean pressure field. For example, Hillier & Cherry (1981) have shown that for smooth flow in the free stream, the maximum value of the mean suction coefficient is smaller in magnitude and occurs further away from the leading edge. Increased levels of free-stream turbulence tend to increase the maximum values of the mean suction coefficients near the leading edge to a significant extent, while moving the location of the maximum closer to the leading edge. However, pressure recovery for the smooth upstream case is slower than for the turbulent case because of the larger reattachment lengths in smooth flow.

Integral scale effects on the mean pressure appear to be more complex. For example, Hillier & Cherry (1981) do not observe any effects of the turbulent integral scales, at fixed levels of turbulence intensity, up to values of $L_x/D = 1.95$. Kiya & Sasaki (1983) and Saathoff & Melbourne (1989) make similar observations. However, the study by Nakamura & Ozono (1987) found that there is dependence of mean pressures over a large range of integral length scales (i.e., over the range of their study with $L_x/D = 0.4$ to 24. For values of L_x/D up to 2, these authors found similar results to those obtained by Hillier & Cherry (1981). However, at larger integral length scales, the mean pressure distribution

begins to behave more like those with smooth upstream flow conditions. The reason for this is that the free-stream fluctuations become relatively slower, with reduced fluctuating energy at the smaller-scales. Thus, these relatively slow fluctuations in the upstream flow are unable to influence the mean flow and the mean pressure over the bodies (Bearman & Morel, 1983; Nakamura & Ozono, 1987) and the combination of both scale and intensity are important parameters for the character of the separation bubble.

1.2 Surface-Mounted, Three-dimensional Bluff Bodies

Many of the engineering applications of bluff body aerodynamics are for buildings, i.e., surface-mounted, three-dimensional prisms, placed in the atmospheric boundary layer. In this case, there are both relatively high turbulence levels along with high levels of mean shear. However, similar flow patterns occur with flow separations, mean flow reattachment and separation bubbles. Despite the similarities in these flow patterns, there are also some significant differences. The main difference arises due to the streamwise vorticity generated in the separated shear layer from the sides of the body (Martinuzzi & Tropea, 1993). For example, Martinuzzi & Tropea (1993) show that, in addition to a recirculation region on the top surface, there is also a recirculation region formed in front of the body (a cube in their particular case). This recirculation region in front of the body extends around the sides of the body, forming a "horseshoe" vortex (Castro & Robins, 1977; Martinuzzi & Tropea, 1993). The aspect ratio of the body is also observed to alter the reattachment lengths. Martinuzzi & Tropea (1993) and Kim *et al.* (2003) both report shorter reattachment lengths for three-dimensional, surface-mounted prisms than those observed for two-dimensional bodies. This is attributed to a mean flow that has a higher acceleration at separation for two-dimensional bodies than for three-dimensional bodies of similar thickness.

So, in contrast to two-dimensional, sharp-edged bluff bodies, the effects of turbulence on surface-mounted bodies have not been systematically investigated. The objective of the present work is to examine the relationships between upstream turbulence conditions on the mean surface-pressure distributions and mean reattachment lengths for relatively low (i.e., with heights less than the plan dimensions), surface-mounted prisms. In order to do so, pressure measurements on two prisms were taken for six different upstream, boundary-layer flows. For one of the prisms (which we will call Building-1), Particle Image Velocimetry (PIV) measurements were made, synchronized with surface pressure measurements. In addition, pressure data from the NIST Low-Rise Building Aerodynamic Database (Ho *et al.*, 2005) are utilized.

2.1 Experimental Set-Up

2.1 Building Models and Pressure Measurements

The dimensions of the two models used in the current study are presented in Table 1. Building-1 is a scaled version of the Texas Tech University "WERFL" Building, which is described in Levitan and Mehta (1992a, b). For this model, a row of 9 pressure taps on the roof surface along the centreline of the building was used. The height of Building-1 is denoted as H_1. A schematic diagram of the models is provided in Figure 2, which also defines the coordinate system. Building-2 is a more generic building, but was previously used in the study by Pratt & Kopp (2014). This was constructed with 96 pressure taps along the centreline. The height of Building-2 is denoted as H_2. Both models were placed

in the high-speed test section of the Boundary Layer Wind Tunnel II at the University of Western Ontario, with the wind direction normal to the wide face for each of the two buildings.

The pressure taps were connected to the pressure scanners by a tubing system, which had a flat frequency response up to about 200 Hz; a complete description of the tubing system can be found in Ho *et al.* (2005). Pressure measurements were taken for approximately 180 seconds at a frequency of 1108 Hz after being low pass filtered at 200 Hz. The pressure measurement system records pressure coefficients referenced to the dynamic pressure at a height of 57 inches from the wind tunnel floor (in a uniform and low turbulence region). These pressure coefficients were converted to obtain the pressure coefficients referenced to dynamic pressure at model height using

$$C_p = Cp_{ref}\left(\frac{V_{ref}}{V_H}\right)^2 \tag{2}$$

Here, Cp_{ref} is the pressure coefficient referenced to the dynamic pressure at the reference height, V_{ref} is the velocity at the reference height, and V_H is the velocity at the model height. Ho *et al.* (2005) demonstrated that pressure coefficients referenced to the dynamic pressure at the model height, which is common wind engineering practice, show the least variability. The uncertainty in the measurements of Cp is dependent on the measurement uncertainties of Cp_{ref}, V_{ref} and V_H. The maximum value of measurement uncertainty in the pressure coefficients referenced to the model height dynamic pressure was observed to be less than 7%, which is controlled by the uncertainty for the square of the velocity ratio in Eq. (2).

Table 1: Model Details.

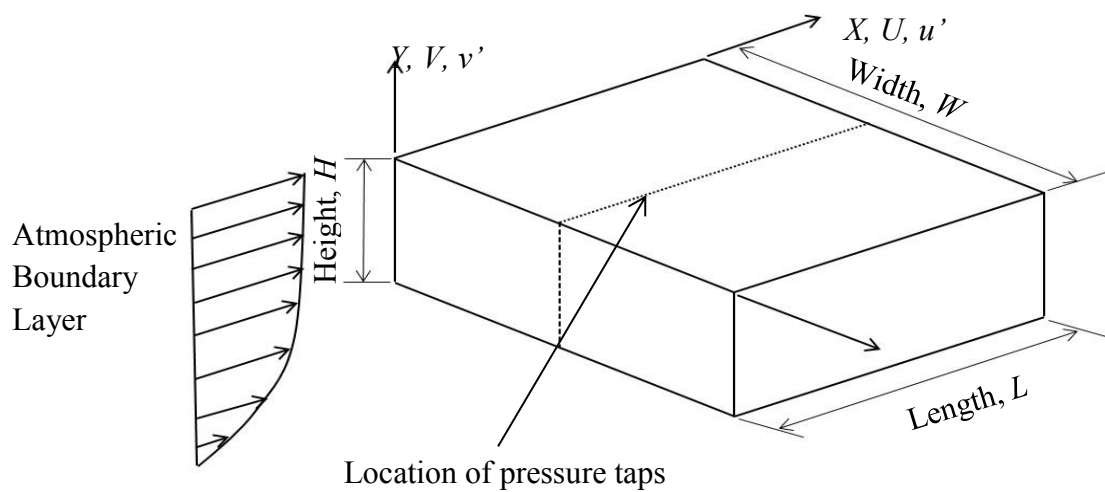| Model Label	Height, H [cm]	Width, W [cm]	Length, L [cm]	Number of pressure taps	Aspect Ratio, AR (=W/H)
Building-1	7.8	27.5	18.4	9	3.5
Building-2	24	75.1	53.3	96	3.1

Figure 2. Schematic diagram of the building models, location of the pressure taps, and coordinate system.

2.2 Terrain Simulation

In wind-tunnel experiments of surface-mounted bluff bodies in deep turbulent boundary layers, characterizing the approaching turbulent boundary layer is important. Such experiments are challenging since proper simulation of atmospheric boundary layers in wind tunnels requires either long and large test sections or small models with small details (Tieleman, 2003). In most boundary layer wind tunnels, the turbulence in the oncoming flow is generated by controlling the heights of roughness elements distributed on the floor of the test section, along with additional turbulence-generating elements, such as spires and barriers, which are usually placed near the entrance of the test section. These roughness elements and turbulence generating elements are chosen in such a way that the desired velocity profiles and turbulence characteristics are achieved. Often the roughness elements are varied in height along the length of the section in order to obtain desired characteristics. During a change in the roughness, an internal boundary layer develops as the flow adjusts. Since it takes time for the turbulence to come into equilibrium with the new roughness (see Tieleman, 2003; Beljaars *et al.* 1983), two distinct regions in the boundary layer are formed with the internal layer growing at slower rate than the outer layer (e.g., Tieleman, 2003). Flow parameters obtained from the lower part of the profile are representative of the local flow characteristics and parameters obtained from the outer part of the profile are representative of flow characteristics over a longer distance upstream (Tieleman, 2003).

Boundary Layer Wind Tunnel II at University of Western Ontario has a high-speed test section that is 3.4 m wide with a nominal height of 2.4 m. The surface of the wind tunnel is provided with surface roughness blocks, which have maximum heights of 200 mm. The high-speed test section is 39 m long from inlet to the centre of the turntable. For the present experiments, a total of six different upstream conditions were developed. These are made up of three different ground roughness configurations, each of which is repeated with and without a 0.38m tall barrier at the test-section inlet. Velocity profile measurements were taken using a Cobra Probe (TFI, Model No. 900311) at a sampling frequency of 1250Hz. The three upstream conditions with the 0.38m tall barrier are labelled as 1L, 2L and 3L while the three without any barrier at the entrance to the test section are labelled as1S, 2S and 3S, i.e., the number in these labels indicates the terrain roughness while "L" indicates the presence of the barrier (and a Larger integral scale) and "S" indicates no barrier (and a Smaller integral scale).

In the velocity profiles for the present experiments, two distinct profile regions are observed because of the presence of the barrier and changes in block heights along the test section length. For all of the upstream conditions, the outer layers were found to be located within a range of heights above the tunnel floor not exceeding 1m from the floor. The velocity measurements only up to the heights of the internal boundary layers are considered and the profile parameters could be obtained by fitting the mean velocity measurements into the logarithmic velocity profile,

$$U = \frac{u^*}{\mathrm{K}}\ln(y) - \frac{u^*}{\mathrm{K}}\ln(y_o) \tag{3}$$

where U is the mean velocity at height, y, from the wind tunnel floor, u^* is the friction velocity, K = 0.41 is the von Karman constant and y_o is the aerodynamic roughness height. Representative velocity and turbulence intensity profiles are shown in Figure 3, in this case for terrain conditions 3S and 3L. It is observed that while both velocity profiles are similar, there is some increase in the turbulence intensity when the barrier is present. However, for some of the other upstream conditions considered here, the roof-height turbulence intensities were not found to be altered significantly due to presence of the barrier. Table 2 provides roof-height turbulence intensities and aerodynamic roughness lengths for each of the six profiles. As can be seen, the inclusion of the barrier increases the integral length scale

6

without substantially altering the turbulence levels or the roughness length, although there are some variations.

Figure 4 shows plots of the velocity spectra for the streamwise and vertical velocity components at height, H_1. These plots confirm that the changes in integral length scale depend primarily on the barrier, while the turbulence intensities and spectral content depend primarily on the terrain roughness, with the barrier increasing the integral scales by up to 100%. The Jensen number, $Je = H/y_o$, is usually used as the scaling parameter for low-rise buildings (Holmes & Carpenter, 1990). Using the measured y_o values, Je values for the current experiments are indicated in Table 2.
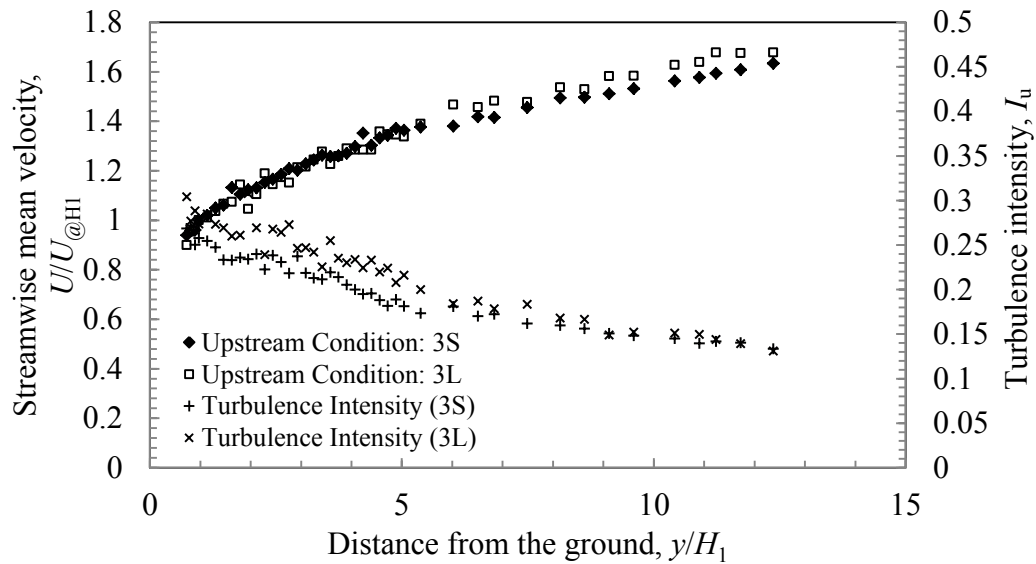

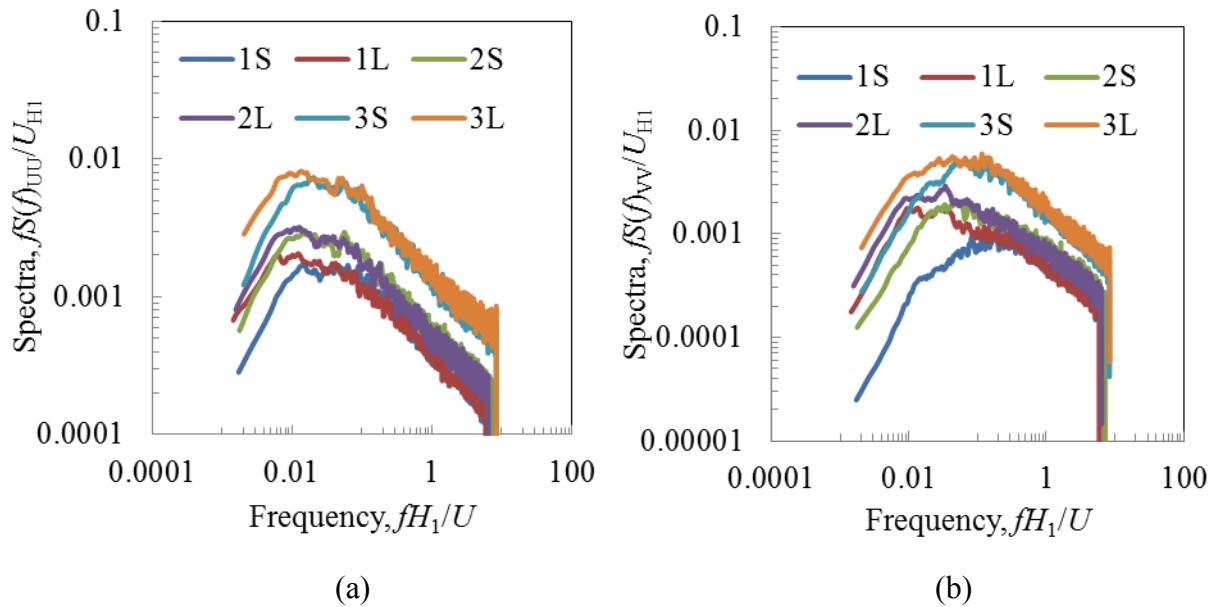Figure 3: Velocity and turbulence intensity profiles for upstream conditions "3S" and "3L".

Figure 4: Velocity spectra at $y = H_1$ for the (a) streamwise, u, and (b) vertical, v, components.

Table 2: Characteristics of the atmospheric Boundary Layer Simulations

Terrain	Barrier [m]	Roughness Length, y_0 [m]	Turbulence Intensity, I_u		Integral Scale, L_x		Jensen Number, J_e	
			$[y = H_1]$	$[y = H_2]$	L_x/H_1	L_x/H_2	$[H_1/y_o]$	$[H_2/y_o]$
1L	0.38	0.00013	14	10	13	4	600	1840
1S	0	0.00014	13	9	6	2	540	1710
2L	0.38	0.00014	17	13	11	5	600	1840
2S	0	0.00027	17	13	8	2	290	890
3L	0.38	0.0011	27	25	12	3.5	71	220
3S	0	0.0014	26	22	7	3	56	170

2.4 Particle Image Velocimetry Measurements

In order to find the mean reattachment lengths on the upper surface of Building-1, the Time Resolved-PIV (TR-PIV) measurements were made. The TR-PIV system has the ability to sample PIV velocity field data at a rate of 500 Hz. Olive oil is atomized, seeded in the flow and illuminated by a double-head, diode-pumped Q-switched Nd:YLF laser operating at a frequency of 1000 Hz. The average pulse energy is 22 mJ. Two 1 Mb Photron FASTCAM-1024PCI CMOS cameras were used to capture the PIV images. A more detailed description of the TR-PIV system can be found in (Taylor *et al.*, 2010). Two fields of view with 20% overlap, one on the upstream side and the other on roof, were selected. Figure 5 shows the photograph of Building-1 placed inside the Boundary Layer Wind Tunnel, the locations of the fields of view and the arrangement of the Time-resolved Particle Image Velocimetry setup. Pressure measurements along the roof centreline were taken for Building-1 with and without placing the particle image velocimetry optics inside the wind tunnel in order to assess the effects of the particle image velocimetry optics on the flow field and surface pressures. The surface pressures were observed to be unaltered by the presence of particle image velocimetry optics inside the wind tunnel. Hence, it can be assumed that the flow fields over the model are also unaffected by the presence of the particle image velocimetry optics.

A time delay of 85μs was applied between the two images of a single image pair so that the particles did not move more than one-fourth of the intended interrogation area. A total of 80000 pairs of PIV raw images of the separated and reattaching flow were captured for each of the six upstream conditions considered in this experiment. TSI Insight 4G, a commercial image processing software package, was used to find the velocity fields, utilizing an FFT cross-correlation algorithm. Interrogation windows of 32x32 pixels with 50% overlap were used during processing the PIV raw images. The post processing on the raw vector data was done by a global standard deviation filter, followed by local mean and median filters. Spurious vectors numbered less than 5% after masking off the visible laser reflection regions and were replaced by interpolated vectors. Standard cross-correlation algorithms have a spatial uncertainty of less than approximately 0.1 pixels (Huang *et al.*, 1997).
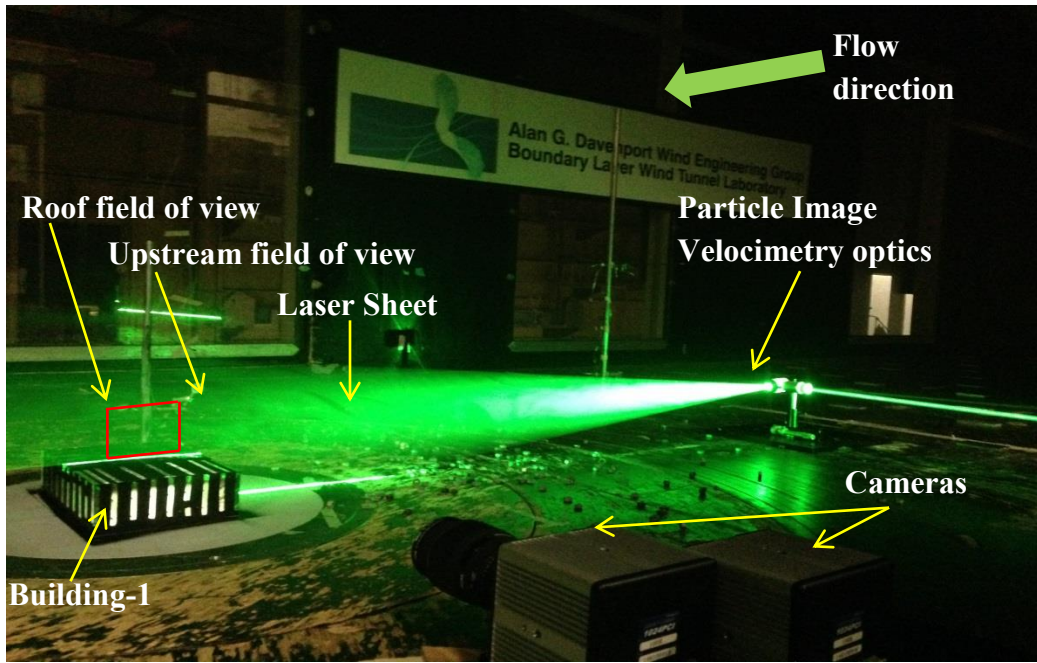
Figure 5: Photograph of experimental set-up, including the arrangement of the Particle Image Velocimetry components and the locations of the fields of view.

3. Mean Reattachment Lengths

3.1 Reattachment Lengths from the PIV Data

The PIV measurements of the flow around Building-1 were taken in order to determine the mean flow field, particularly the reattachment lengths and locations of the stagnation points. Figure 6 shows the mean streamlines around Building-1 for one upstream condition, 2L. From the figure it can be seen that the flow separates at the edge of the roof and reattaches downstream between 1.0 to 1.1H. The mean reattachment points for all six upstream conditions for Building-1 were obtained by identifying the point on the roof surface where the flow changes direction (from reverse to the forward flow). The uncertainties associated with these measurements mainly arise due to lack of velocity data in the masked-off regions (because of laser reflections from the surface) and due to the resolution of the PIV measurements, which have a spacing of 0.02H_1. The uncertainties in the measurements of mean reattachment lengths (Xr) due to masked off regions near the surface and vector spacing are estimated to be within a range of 3% to 5% of X_r. Table 3 provides the mean reattachment lengths with the corresponding upstream flow properties. Note that the sizes of the reattachment lengths for the "1L" and "1S" conditions were large enough that they extended beyond the field of view of the PIV camera. In these cases, the reattachment points were approximated by extrapolating the streamlines along the centre of the separated shear layer, which obviously increases the uncertainty for these points.

From Table 3, it can be seen that, for higher levels of the streamwise turbulence intensity, the mean reattachment length is smaller. For example, there is a reduction of about 35% in the reattachment length when the turbulence intensity is changed from 12% to 26% (from upstream condition "1L" to "3S"). A closer look at the data reveals that integral length scales do not significantly affect the mean reattachment length over the range examined. Noting that the spectra are similar for each terrain configuration, this result appears to be consistent with the findings of Hillier and Cherry (1981) over the limited range of tested integral scales.
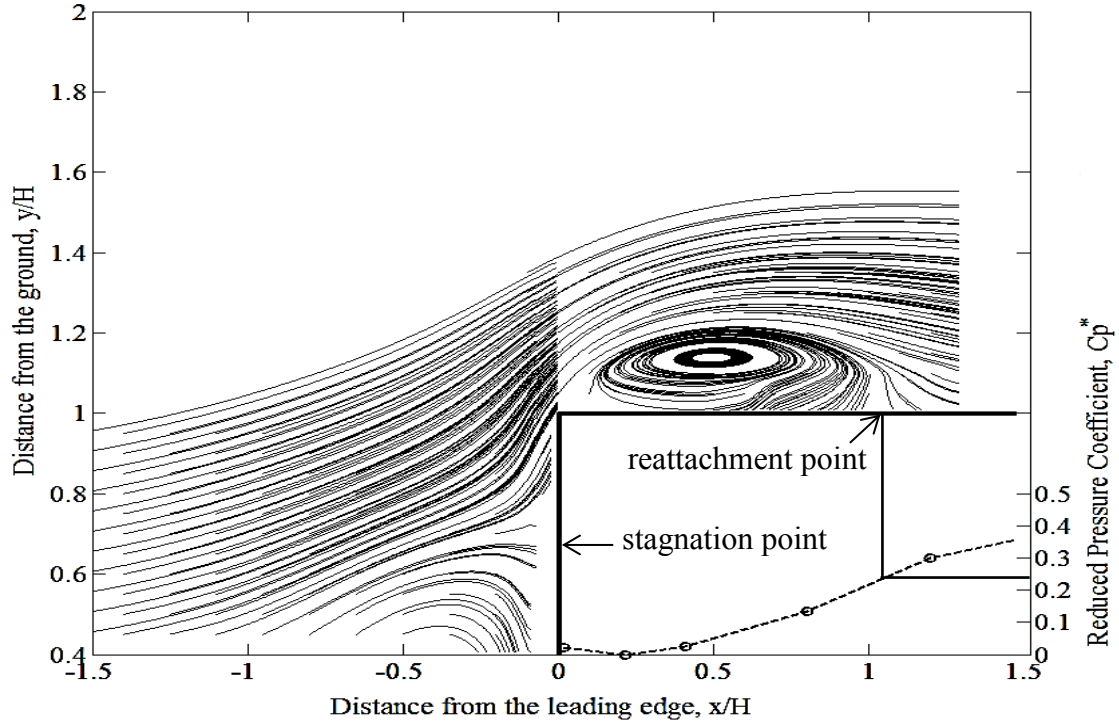
Figure 6. Mean streamlines around Building-1 for upstream condition 2L, along with the distribution of reduced pressure coefficients (Cp^*) on the roof.

In addition to the reattachment length on the roof, the location of the stagnation point on the front face of Building-1 is necessary in order to compare reattachment lengths with those from two-dimensional bluff bodies. It is the distance from the stagnation point to the roof edge that is the important geometric length scale (Hillier & Cherry (1981), Kiya & Sasaki (1983), Saathoff & Melbourne (1997)). It is observed that, irrespective of the flow details, the mean location of the front-face stagnation point is at $y = 0.65H_1$ in the current experiments. Thus, the distance from the stagnation point to the roof edge, $h_f = 0.35H$ for these surface-mounted bodies. This contrasts with $h_f = 0.5H$ for two-dimensional bodies (of total height H) in a uniform stream. In addition, from the present experimental results, the upstream turbulence levels and scales do not appear to have significant influence on the height of the stagnation point above the ground plane. The experimental results of Kim *et al.* (2003) for a surface-mounted, three-dimensional prism with a roof height turbulence level of 20% show that the location of the stagnation point on the front surface of the model is at $0.7H$ from the ground plane, indicating a reasonable consistency between the two studies.

10

Table 3. Mean reattachment lengths, X_r, obtained via PIV measurements for Building-1.

Upstream Condition	$(I_u)_{H1}$ (%)	L_x/H_1	X_r/H_1
1L	14	13	~1.4
1S	13	6	~1.4
2L	17	11	1.05
2S	17	8	1.05
3L	27	12	0.88
3S	26	7	0.88

3.2. Mean Reattachment Lengths from Pressure Data

Eq. (1) was first proposed by Roshko & Lau (1965) as an appropriate normalization of the pressure distribution within separation bubbles. Ruderich & Fernholz (1986) showed that, for separating – reattaching flows, irrespective of the blockage ratios and Reynolds numbers, when the reduced pressure coefficients are plotted against the distance from the leading edge normalized by the mean reattachment length, there is similarity of the profile. Using their own experimental results, along with a series of results obtained from literature, Hudy *et al.* (2003) showed that there is a constant value of reduced pressure coefficient of 0.35 at the reattachment point. The dataset considered in their analysis were for two-dimensional bluff bodies with relatively long reattachment lengths (e.g., the maximum X_r/h_f being 33.6 and the minimum being 4.9) and with a maximum turbulence intensity of 4% (and the maximum Reynolds number of 3.2×10^4). For the present experiments on surface-mounted prisms, the upstream conditions have much higher turbulence intensities, ranging from 9% to 27% with the size of the separation bubbles being small compared to the data considered by Hudy *et al.* (2003). Hence, the present experiments are rather different from the data considered previously. This leads to some different outcomes, as discussed below.

Figure 6 depicts the distribution of the reduced pressure coefficients, Cp^*, as defined in Eq. (1) for the roof of Building-1 in upstream terrain condition 2L, along with the mean streamlines. Comparing the pressure distribution with the location of the reattachment point, it is observed that Cp^* = 0.24 at reattachment for this terrain configuration. Using the observed reattachment points from the PIV data, the reduced pressure coefficient, Cp^*, distributions are plotted versus x/X_r for the six terrain configurations in Figure 7. It can be observed that the distributions of the reduced pressure coefficients are broadly similar between the six cases, although there are significant differences in magnitudes of the reduced coefficients. There are also significant differences when compared to the distributions found by Ruderich & Fernholz (1986) and Hudy *et al.* (2003) for uniform, low turbulence flow. The minimum value of the mean pressure coefficient, and of Cp^*, occurs near x/X_r = 0.25, after which the pressure recovers, with Cp^* increasing to values between 0.2 and 0.3 at reattachment point. These data indicate that, at the reattachment point, the values of Cp^* depend on the upstream conditions. In fact, increasing the turbulence intensity appears to reduce the value of Cp^* at x/X_r = 1 so that it has a value of about 0.2 for I_u = 26-27%, about 0.3 at I_u = 13-14%, and about 0.35 in the smooth flow data of Ruderich & Fernholz (1986) and Hudy *et al.* (2003). Considering the distributions in Figure 7, it appears that the integral scales in the upstream flow do not have significant effect on the value of Cp^* at the reattachment point, at least over the range tested. Thus, the normalized pressure distribution in separation bubble appears to depend significantly on the turbulence level in the free stream.
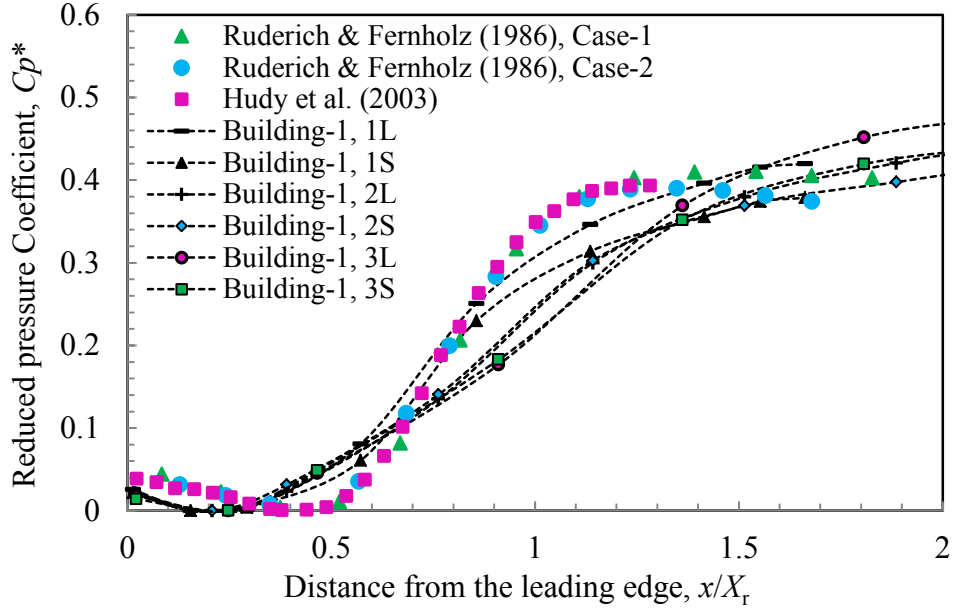
Figure 7: Distribution of reduced pressure coefficient (Cp^*) for Building-1.

Figure 8 shows the variation of reduced pressure coefficients at the reattachment point versus the roof-height turbulence intensities for Building-1. Included in the graph are also the results of Ruderich & Fernholz (1986) and Hudy *et al.* (2003) (for two-dimensional bodies in low turbulence). While the true functional variation of Cp^* at $x/X_r = 1$ is unknown, it is approximated here with a linear equation, also shown on the figure. It is observed that the fit satisfactorily approximates the variation of reduced pressure coefficients at the mean reattachment point for Building-1. Using the fitted linear equation, the reattachment lengths are estimated and presented in Table 4 along with the error in the estimates. As can be seen, the errors are reasonably small and similar to the measurement uncertainty for the pressure coefficients. (It should also be noted that an extension of the linear fit nearly falls on the data of Hudy *et al*. (2003), which has turbulence levels of up to 4%. Further research is required to establish whether or not this is fortuitous.)

Since the errors and uncertainties from using Cp^* to estimate X_r appear to be reasonably small, the linear fit from Figure 8 is used to estimate the reattachment lengths for Building-2. Table 4 presents these values, which will be examined in greater detail below. In addition to the current data, the wind tunnel pressure data stored by the National Institute of Standards and Technology (NIST) were analyzed. This database, which is described in detail by Ho *et al.* (2005), contains a series of measured surface pressures building models of different heights, plan dimensions and gable-roof slopes for two different upstream terrain conditions. From the NIST dataset only the data for slope of the roof less than or equal to 1:12 (i.e., 4.8°) were extracted in order to compare with present experiments. The mean reattachment lengths were estimated based on the values provided by Figure 8, along with the measured roof-height turbulence intensities. These values are reported in Table 5 and will also be examined in greater detail below.
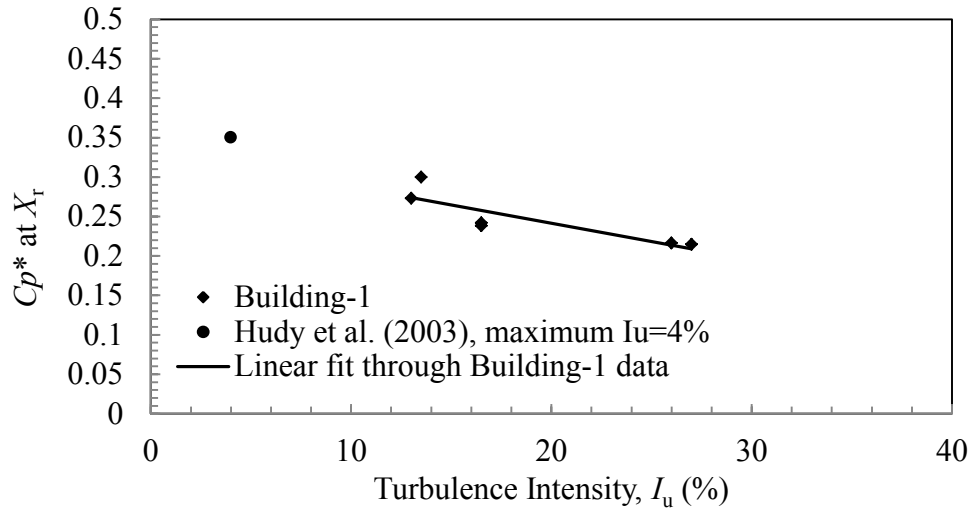
Figure 8: Variation of the reduced pressure coefficient, Cp^*, at the reattachment point with turbulence intensity, I_u.

Table 4: Estimated reattachment lengths, X_r, for Building-1 and Building-2 using the fit from Figure 8.

| Terrain	$(I_u)_{H1}$	L_x/H_1	X_r/H_1 (error)	Cp^* at X_r Building-1 (directly measured)	$(I_u)_{H2}$	L_x/H_2	C_p^* at X_r Building-2	X_r/H_2
1L	14	13	1.29 (-3.9%)	0.27 (0.30)	10	4	0.31	1.49
1S	13	6	1.42 (+0.7%)	0.28 (0.28)	9	2	0.32	1.50
2L	17	11	1.09 (+1.8%)	0.25 (0.24)	13	5	0.28	1.12
2S	17	8	1.08 (+1.3%)	0.25 (0.24)	13	2	0.28	1.18
3L	27	12	0.87 (-0.5%)	0.21 (0.21)	25	3.5	0.22	0.62
3S	26	7	0.87 (-0.5%)	0.21 (0.21)	22	3	0.23	0.67

Table 5: Flow characteristics and estimated mean reattachments lengths for buildings from the NIST dataset (Ho *et al.*, 2005). All dimensions are in the stated full-scale dimensions; the roof slope is 1:12 unless otherwise stated. Open terrain is a roughness length of $y_o = 0.03$m; suburban terrain is $y_o = 0.3$m.

| H [m]	Plan dimensions [m x m]	$(I_u)_H$ (open)	X_r/H, Open Terrain (estimated)	$(I_u)_H$ (suburban)	X_r/H, Suburban Terrain (estimated)	$\Delta X_r/H$ [%]	Symbol in Fig. 11 (open)	Symbol in Fig. 11 (suburban)
3.7	19x12	20	0.65	28	0.52	20.1	▽ (green)	▼ (green)
5.5	19x12	19	0.66	27	0.56	14.7	▽ (blue)	▼ (blue)
7.3	19x12	19	0.7	26	0.55	21.6	▽ (red)	▼ (red)
12.2	19x12	18	0.71	25	0.47	33.8	▽ (magenta)	▼ (magenta)
4.9	38x24	19	0.93	27	0.75	20.2	□ (green)	■ (green)
7.3	38x24	19	0.81	26	0.65	20.2	□ (blue)	■ (blue)
9.8	38x24	18	0.72	25	0.59	18.6	□ (red)	■ (red)
12.2	38x24	18	0.69	25	0.54	22.2	□ (magenta)	■ (magenta)
5.5	38x24 (roof slope 1:48)	19	1.11	27	0.86	22.4	◇ (green)	◆ (green)
7.3	38x24 (roof slope 1:48)	19	1.03	26	0.78	24.1	◇ (blue)	◆ (blue)
9.8	38x24 (roof slope 1:48)	18	0.94	25	0.72	23.9	◇ (red)	◆ (red)
12.2	38x24 (roof slope 1:48)	18	0.9	25	0.65	28.0	◇ (magenta)	◆ (magenta)
3.7	57x36	20	1.01	28	0.86	14.7	○ (magenta)	● (magenta)
4.9	57x36	19	0.97	27	0.8	17.2	○ (black)	● (black)
5.5	57x36	19	0.92	27	0.76	17.5	○ (green)	● (green)
7.3	57x36	19	0.92	26	0.69	24.9	○ (blue)	● (blue)
12.2	57x36	18	0.75	25	0.56	24.6	○ (red)	● (red)
5.5	76x48	19	1	27	0.73	26.9	△ (green)	▲ (green)
7.3	76x48	19	0.92	26	0.71	23.3	△ (blue)	▲ (blue)
12.2	76x48	18	0.78	25	0.57	27.7	△ (red)	▲ (red)

3.3 Effects of Aspect Ratio

Aspect ratio, defined as the width-to-height ratio, i.e., $AR = W/H$, is a parameter that is also known to affect mean reattachment lengths. For example, Gu & Lim (2012) show that for an incremental increase of the aspect ratio for surface-mounted prisms, mean suction coefficients increase and the pressure recovery is delayed. Cherry $et\ al.$ (1984) found that increasing the aspect ratio of bluff bodies in a uniform stream increases the reattachment length up to the point when an asymptotically-limiting value is reached. However, they also found that the asymptotically-limiting aspect ratio depends on blockage ratio.

Figure 9 depicts the variation of mean reattachment lengths (X_r/h_f) as a function of aspect ratios for the NIST data obtained for the "open" (with an average roof height turbulence intensity of 19%) and "suburban" (with an average roof height turbulence intensity of 26%) terrains, with 1:12 and 1:48 roof slopes. Since the flow field was not measured for these cases, the explicit assumption that the Cp^* value at X_r versus I_u relationship from Figure 8 holds for these data and is not altered by the aspect ratio. Several observations can be made. First, there is clearly scatter in the plots, which may be due to the pressure tap resolution for the NIST data, in addition to measurement uncertainty, and variations and errors associated with the relationship between Cp^* at $x = X_r$ and the turbulence intensity (Figure 8). Second, from Figure 9(a), for gable-roofed buildings with 1:12 roof slope, it is observed that for turbulence intensities consistent with an open terrain, increasing the aspect ratio increases the mean reattachment length. This relationship can be described satisfactorily by an exponential equation (with an upward trend), although there is substantial extrapolation to the asymptotic limit. For the higher level of turbulence intensity characteristic of a suburban terrain, the variation of mean reattachment length with aspect ratio follows a similar trend. In fact, both fits are nearly parallel to each other. Similar observations can also be made from the data presented in Figure 9(b) for gable roofs with 1:48 roof slopes. Third, it is estimated that for both upstream conditions, the asymptotic limit of the mean reattachment length occurs at aspect ratios between 50 and 80 (considering the asymptotic limit as 99% of maximum value of X_r) for 1:12 and 1:48 roof slopes. Finally, Figures 9(a) and 9(b) indicate that X_r/h_f is ~0.5 larger for the flatter roof slope of 1:48, when compared the more-highly sloped 1:12 data.
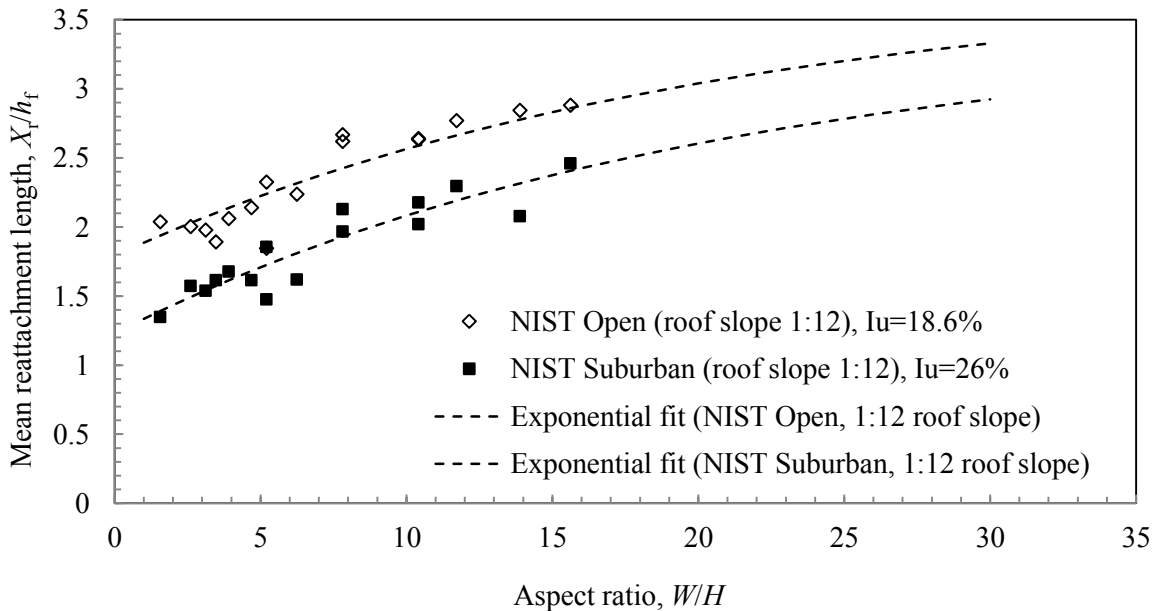
(a)
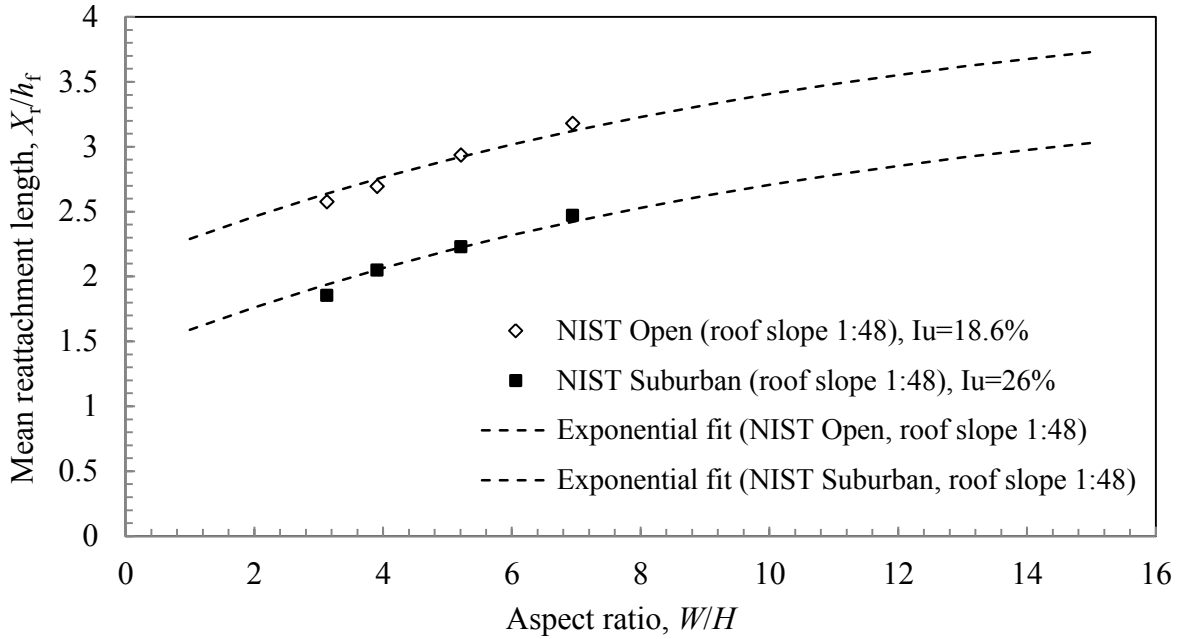
(b)

Figure 9: Variation of mean reattachment length with aspect ratio for NIST data for roof slopes of (a) 1:12 and (b) 1:48.

3.4 Discussion

In order to compare experimental data for different aspect ratios, it is necessary to adjust the results to a common aspect ratio and roof slope. Here we choose to use the asymptotic limit and the 1:48 roof slope so that the reattachment lengths for the current, three-dimensional, surface-mounted prisms can be compared to two-dimensional prisms in uniform flow. Thus, the reattachment lengths were converted to those for the asymptotic-limit. These are plotted in Figure 10 as a function of turbulence intensity. Included in Figure 10 are the results from Saathoff & Melbourne (1997) for two-dimensional bluff bodies placed in four uniform flows with different upstream turbulence levels and the results obtained by Kim *et al.* (2003) for a surface-mounted, three-dimensional prism with a 20% roof-height turbulence intensity (and also modified to account for aspect ratio).

Several observations can be made. First, as discussed above, there is a strong trend for decreasing reattachment lengths with increasing turbulence intensity. Most of the changes occur for $I_u < \sim17\text{-}18\%$, with relatively little change in the reattachment lengths for larger values of I_u. In fact, the range of the scatter is greater than the underlying trend for $I_u > \sim17\text{-}18\%$.

Second, it appears that surface-mounted prisms have a different trend-line than those placed in a uniform stream with the reattachment lengths for surface-mounted prisms being larger at the turbulence intensities where there is overlap. It should be emphasized that there is considerable uncertainty in the extrapolation to large aspect ratio for the surface-mounted bodies, with the largest aspect ratios being about 16 in the experiments. Nevertheless, the evidence suggests that the curve for true two-dimensional bodies in a uniform stream is distinct from that for three-dimensional surface-mounted bodies extrapolated to large aspect ratios. While the uniform flow results end at $I_u = 15\%$, it appears that the uniform flow data and the current data have similar magnitudes beyond this point; however, there are no data to examine this point further. At lower turbulence intensities, it appears that the trend-lines for the two classes of bluff bodies are diverging, with larger reattachment lengths for the surface-

16

mounted prisms. However, the first data point is at only $I_u = 9\%$. It seems likely that this difference is due to the nature of the vortical structures formed around surface-mounted prisms, which do not exist for two-dimensional bodies in a uniform stream, as discussed in the Introduction, although it could be due to other differences including the effects of the mean shear and anisotropic turbulence of the atmospheric boundary layer. Since the streamwise dimension of the surface-mounted low-rise building is comparatively small (e.g., L/H=2.36 for Building-1), the interaction between vortices shed at the trailing edge with the separation bubble may also have some effect on the mean reattachment length for surface-mounted three-dimensional bluff bodies, and the underlying assumptions for the aspect ratio corrections. These points merit further study in future work.
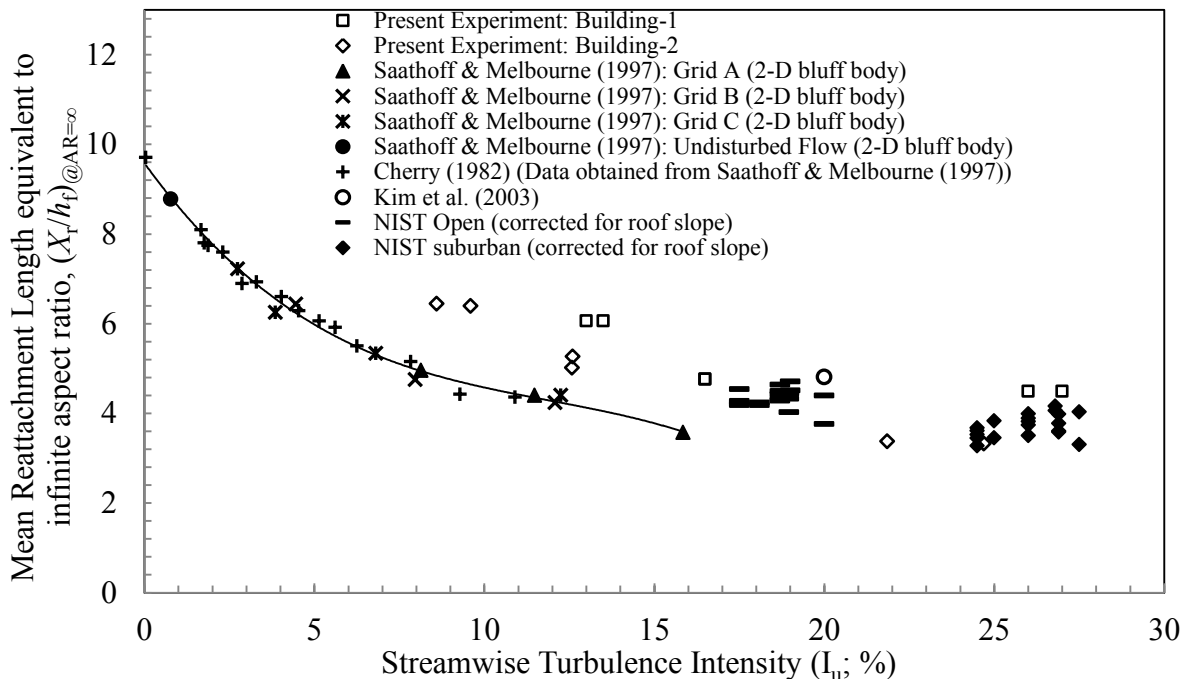

Figure 10: Variation of mean reattachment length, corrected to infinite aspect ratio, $(X_r/h_f)_{@AR=\infty}$, as a function of streamwise turbulence intensity. A polynomial fit through the 2D bluff-body data is also shown for clarity.

4. Mean Pressure Distribution

Having established the variation of the reattachment length as a function of aspect ratio and turbulence intensity, we re-visit the normalization of the mean pressure distribution via Eq. (1). Figure 7 shows the variation of the reduced pressure coefficient, Cp^* versus x/X_r for Building-1. As discussed above, the value of Cp^* at $x/X_r = 1$ varies significantly (Figure 8). Adding to Figure 7, the Building-2 and NIST data are included, based on the model for the reattachment lengths indicated by Figure 8. The results are shown in Figure 11.

Figure 11, indicates that there is dependence of the reduced pressure curves on the turbulence intensity. The clear trend of larger values of Cp^* for smaller I_u values is apparent, notwithstanding the scatter in these plots. In general, those having similar levels of turbulence have similar shapes and magnitudes, although they do not fall perfectly onto a single curve. These results, when compared to

17

those of Hudy *et al.* (2003) and Ruderich and Fernholz (1986), are clearly different. Thus, one can conclude that the normalized pressure distributions depend on more than distance normalized by the reattachment length, with the turbulence intensity significantly affecting the normalized distribution. Given the variations in the curves, other parameters (such as integral scales) must also affect the distributions, but to a lesser extent. In general, the pressure begins to recover earlier, i.e., at smaller x/X_r values (i.e., $x/X_r \sim 0.2$ to 0.3 compared to $x/X_r \sim 0.4$ to 0.5 for low turbulence) but beyond this point, the turbulence level slows the pressure recovery so that there are significantly lower values of Cp^* at the reattachment point. So, while higher levels of turbulence intensity reduce the reattachment length, the mean pressure on the surface does react as quickly resulting in lower Cp^* values at reattachment.

While Figure 11 highlights the changes in the normalized pressure distribution, it should also be noted that Cp_{min} varies significantly, depending on the turbulence intensity. For both buildings measured in the current study, it is observed that the minimum pressure coefficient for all of the upstream conditions falls between values of -0.9 to -1.3 with the lower values occurring at the higher turbulence intensities. Following reattachment, the pressure drop is nearly recovered with values of the pressure coefficient between -0.1 and -0.2 for these experiments. Figure 12 depicts the Cp_{min} values (along with a curve fit). The data show quite a lot of scatter, although the trend is clearly discernible, consistent with other experimental observations (e.g., Castro & Robins, 1977; Tieleman *et al.*, 1996) and the measurement uncertainty.
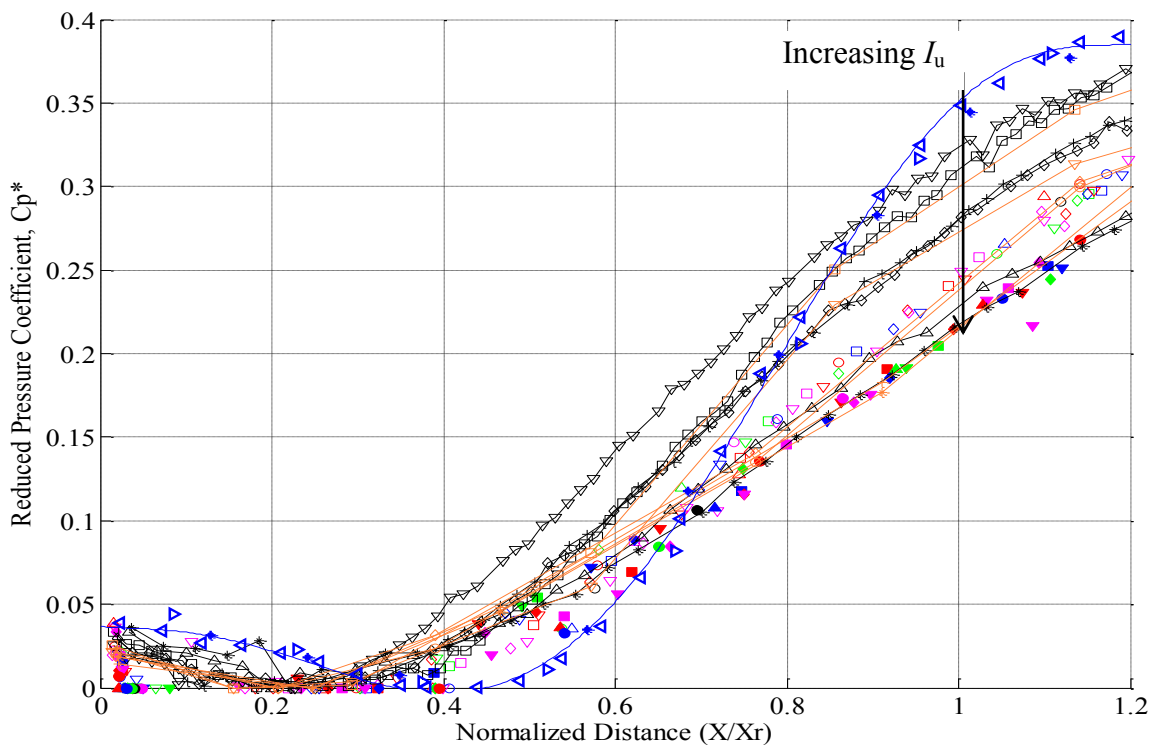

Figure 11. Distribution of the reduced pressure coefficient (C_p^*) under the separation bubble. Legends: Building-1: 1L ; 2L ; 3L ; 1S ; 2S ; 3S ; Building-2: 1L ; 2L ; 3L ; 1S ; 2S ; 3S ; Hudy *et al.* (2003) ; Ruderich & Fernholz (1986), Case-1 ; Ruderich & Fernholz (1986), Case-2 ; polynomial fit through the Hudy et al. (2003) and Ruderich & Fernholz (1986) ; NIST data legends are listed in Table 5.
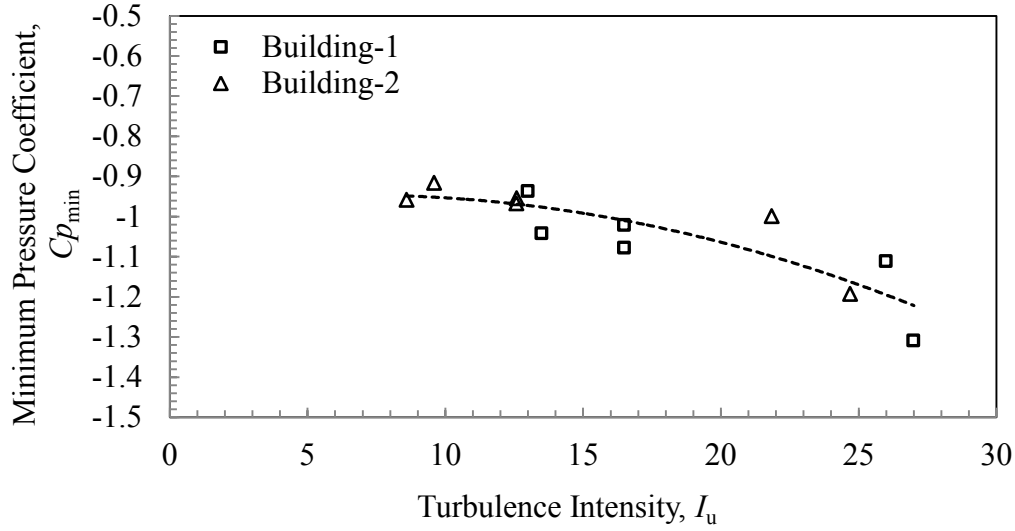
Figure 12: Variations of minimum mean pressure coefficient with turbulence intensities. A polynomial fit through the dataset of Building-1 and Building-2 are shown on the figure with a dashed curve.

5. Discussion

From the Particle Image Velocimetry and surface pressure data for Building-1 it is observed that the building height turbulence intensity in the upstream boundary layer flow is the key turbulence parameter affecting the size of the separation bubble. For the range of turbulence length scales considered in this experiment (L_x/H = 6 to 13), no significant effect of turbulence length scales on the size of the separation bubble was observed. However, for very large values of integral scales in the upstream boundary layer, similar effects may not be observed. For two-dimensional bluff bodies placed in uniform upstream flows, it is observed in the literature that, at significantly larger values of turbulence length scale (relative to the body thickness, L_x/H), the surface mean pressure distributions behave more like smooth upstream flow over bluff bodies (Nakamura & Ozono, 1987). Bearman & Morel (1983) and Nakamura & Ozono (1987) suggest that, at these large values of upstream scales, the slowly fluctuating velocities are unable to alter the mean flow inside the separation bubble and that this may lead to larger separation bubbles. For surface-mounted bodies, similar effects would be expected.

For a fixed turbulence intensity, larger integral scales imply lower energy levels at the higher frequencies (smaller scales). Consider, for example, the von Kármán spectrum,

$$\frac{fS_{uu}}{\sigma^2} = \frac{4\left(\frac{L_x f}{\bar{u}}\right)}{\left[1+70.8\left(\frac{L_x f}{\bar{u}}\right)^2\right]^{5/6}}$$

(4)

which indicates that the normalizing parameters for the power spectral density of the streamwise velocity are the variance, σ^2, and the integral time scale, $L_x/\bar{u}$. One can re-write this in terms of the turbulence intensity and L_x/H,

$$\frac{fS_{uu}}{\bar{u}^2} = \frac{4\left(\frac{L_xf}{\bar{u}}\right)I_u^2}{\left[1+70.8\left(\frac{L_xf}{\bar{u}}\right)^2\right]^{5/6}} \qquad (5)$$

Figure 13 illustrates the spectra for $H = 4$m and $\bar{u} = 30$m/s. For the spectrum with $L_x/H = 200$ and $I_u = 17\%$, the energy is shifted to larger wavelengths relative to the size of the building compared to the spectrum with $L_x/H = 10$ and $I_u = 17\%$. At wavelengths similar to the building size, i.e., $fH/\bar{u} \sim 1$ there is an order of magnitude more energy for $L_x/H = 10$ than for $L_x/H = 200$. While this undoubtedly affects the fluctuating pressures, one may also expect a change towards lower-turbulence-level (i.e., smoother) mean-flow results, based on the Nakamura & Ozono (1987) data. Quasi-steady theory results suggest that the cut-off for "passive" fluctuations is at about $fH/\bar{u} \sim 0.1$ (e.g., Wu & Kopp, 2016, for a building with the same geometry as Building-1). If this holds generally, then the $L_x/H = 200$, $I_u = 17\%$ flow would yield similar aerodynamics (i.e., similar reattachment lengths and pressure distributions) as for the $L_x/H = 2$ and $I_u = 4\%$ spectrum shown in Figure 13. This is the argument made by Irwin (2008; see his Figure 9) regarding the "partial turbulence simulation" method. Clearly, such results would have significant implications on how scale-model wind tunnel tests are conducted, particularly for large model scales.
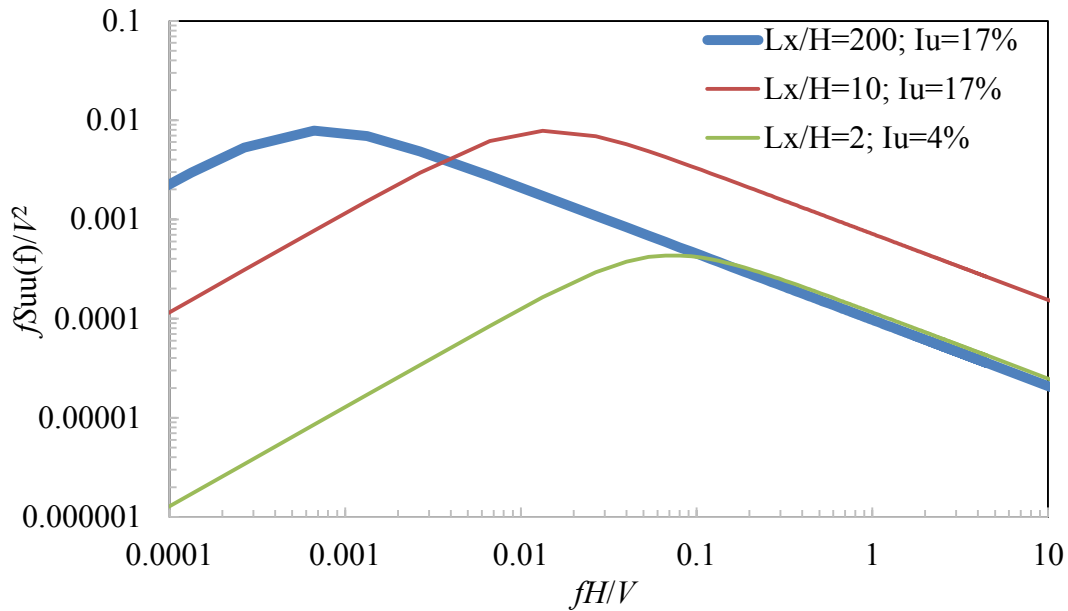

Figure 13. Streamwise velocity spectra for $H = 4$m and $\bar{u} = 30$m/s and various integral scales and turbulence intensities.

For low-rise buildings in the range from $H = 4$m to 20m, in open ($I_u \sim 17\%$) or suburban ($I_u \sim 27\%$) terrain, L_x/H is in the range from 7 to 33, based on the integral scales found by Counihan (1975) for the atmospheric boundary layer. The experiments for Building-1 are within this range (but do not fully span it). Thus, the current data for Building-1 (i.e., Tables 3 and 4 and Figures 7 and 8) are of practical relevance for typical wind engineering applications for low-rise buildings. In general, further research is required to more fully assess the impact of integral scales outside the range tested, although it should be emphasized that there are challenges with respect to the size of boundary layer wind tunnels

achieving larger integral scales relative to reasonably sized building models, as discussed by Tieleman (2003).

6. Conclusions

The objective of the paper is to examine the effects of turbulence intensity and scale in upstream boundary layers on the mean reattachment length and pressure distributions for low-rise buildings. PIV and surface pressure measurements were made on a model building in six distinct terrain simulations, along with a detailed analysis of the pressure measurements from another low-rise building model for similar six terrains. The roof centre-line pressure for low-rise buildings with roof slopes less than or equal to 1:12 extracted from the NIST dataset (Ho *et al.*, 2005) were also utilized in the analysis. The following conclusions can be drawn from the results:

➢ The mean location of the stagnation streamline on the front wall of a low rise building is found to be at 0.65H and is unaffected by the turbulence properties in the upstream flow.

➢ The mean reattachment length is primarily dependent on the streamwise turbulence intensity upstream of the building and the building aspect ratio. For the low-rise building models considered in the present experiment, it is seen that increasing the roof height turbulence intensities causes the mean reattachment lengths to decrease. For instance, increasing roof height turbulence from I_u = 9% to 25% reduced the size of the separation bubble by more than 30%.

➢ It was found that the reduced pressure coefficient, Cp^*, distribution within separation bubbles depends primarily on the reattachment length, but also depends on the turbulence intensity. Values of Cp^* at x/X_r = 1 range from about 0.35 for low turbulence (from Hudy *et al.*, 2003) to about 0.20 at $I_u \sim 25\%$. Thus, while high turbulence levels cause earlier reattachment, the pressure does not recover at the same rate, relative to the reattachment point.

➢ Larger aspect ratios also yield larger mean reattachment lengths. For example, with $I_u \sim 18\%$, changing the aspect ratio from 2 to 16 increased the reattachment length by about 50% under the assumption that the Cp^* value at reattachment is unaltered by aspect ratio. Further research is required to confirm this point.

➢ The reattachment length was found to be largely unaffected by the integral length scales over the range of values examined (i.e., L_x/H = 6 to 13). However, for significantly larger integral scales, the reattachment length is also expected to be an important parameter.

7. Acknowledgements

References

Bearman, P. W. and Morel, T. 1983 Effects of free stream turbulence on the flow around bluff bodies. *Progress in Aerospace Science*. **20**, 97-123.

Beljaars, A. C. M., Schotanus, P. and Nieuwstadt, F.T.M. 1983 Surface layer similarity under nonuniform fetch conditions. *Journal of Climate and Applied Meteorology*. **21**, 1800–1810.

Castro, I. P. and Robins, A. G. 1977 The flow around a surface-mounted cube in uniform and turbulent streams. *Journal of Fluid Mechanics*. **79**, 301-335.

Cherry. N. J., Hillier, R. and Latour, P. M. 1984 Unsteady measurements in a separated and reattaching flow. *Journal of Fluid Mechanics*. **144**, 13-46.

Counihan, J. 1975 Adiabatic atmospheric boundary-layers: A review and analysis of data from the period 1880-1972. *Atmospheric Environment*. **9**, 1-35.

Gartshore, I. S. 1973 The effects of free stream turbulence on the grad of rectangular two-dimensional prisms. *University of Western Ontario*. BLWTL-**4**-73.

Gu, D. and Lim, H. C. 2012 Wind flow around rectangular obstacles and the effects of aspect ratio. *The Seventh International Colloquium on Bluff Body Aerodynamics and Applications (BBAA7)*. Shanghai, China; September 2-6.

Hillier, R. and Cherry, N. J. 1981 The effects of stream turbulence on separation bubbles. *Journal of Wind Engineering and Industrial Aerodynamics*. **8**, 49-58.

Ho, T. C. E., Surry, D., Morrish, D. and Kopp, G. A. 2005 The UWO contributions to the NIST aerodynamic database for wind loads on low buildings: Part1. Archiving format and basic aerodynamic data. *Journal of Wind Engineering and Industrial Aerodynamics*. **93**, 1-30.

Holmes, J. D. and Carpenter, P. 1990 The effects of Jensen number variations on the wind loads on a low-rise building. *Journal of Wind Engineering and Industrial Aerodynamics*. **36**, 1279-1288.

Huang, H., Dabiri, D. and Gharib, M. 1997 On errors of digital Particle Image Velocimetry. *Measurement Science and Technology*. **8**, 1427-1440.

Hudy, L. M, Naguib, A. M. and Humphreys, W. M. Jr. 2003 Wall-pressure-array measurements beneath a separating/reattaching flow region. *Physics of Fluids*. **15(3)**, 706-717.

Irwin, P.A., 2008 Bluff body aerodynamics in wind engineering. *Journal of Wind Engineering and Industrial Aerodynamics*. **96**, 701.

Kim, K. C., Ji, H. S. and Seong, S. H. 2003 Flow structure around a 3-D rectangular prism in a turbulent boundary layer. *Journal of Wind Engineering and Industrial Aerodynamics*. **91**, 653-669.

Kiya, M. and Sasaki, K. 1983 Free stream turbulence effects on a separation bubble. *Journal of Wind Engineering and Industrial Aerodynamics*. **14**, 375-386.

Levitan, M.L. and Mehta, K.C. 1992a Texas Tech field experiments for wind loads. Part 1: Building and pressure measuring system. *Journal of Wind Engineering and Industrial Aerodynamics*. **43**, 1565.

Levitan, M.L. and Mehta, K.C. 1992b Texas Tech field experiments for wind loads. Part 1: Meteorological instrumentation and terrain parameters. *Journal of Wind Engineering and Industrial Aerodynamics*. **43**, 1577.

Lyn, D. A. and Rodi, W. 1994 The flapping shear layer formed by flow separation from the forward corner of a square cylinder. *Journal of Fluid Mechanics*. **267**, 353-376.

Martinuzzi, R. and Tropea, C. 1993 The flow around surface-mounted, prismatic obstacles placed in a fully developed channel flow. *Journal of Fluids Engineering*. **115**, 85-92.

Nakamura, Y. and Ozono, S. 1987 The effects of turbulence on a separated and reattaching flow. *Journal of Fluid Mechanics*. **178**, 477-490.

Pratt, R. N. and Kopp, G. A. 2014 Velocity field measurements above the roof of a low-rise building during peak suctions. *Journal of Wind Engineering and Industrial Aerodynamics*. **133**, 234-241.

Ruderich, R. and Fernholz, H. H. 1986 An experimental investigation of a turbulent shear flow with separation, reverse flow, and reattachment. *Journal of Fluid Mechanics*. **163**, 283-322.

Roshko, A. and Lau, J. C. 1965 Some observations on transition and reattachment of a free shear layer in incompressible flow. *In Proceedings of the 1965 Heat Transfer and Fluid Mechanics Institute*.

Saathoff, P. J. and Melbourne, W. H. 1989 The generation of peak pressures in separated/reattaching flow. *Journal of Wind Engineering and Industrial Aerodynamics*. **32**, 121-134.

Saathoff, P. J. and Melbourbe, W. H. 1997 Effects of free stream turbulence on surface pressure fluctuations in a separation bubble. *Journal of Fluid Mechanics*. **337**, 1-24.

Taylor, Z. J., Gurka, R., Kopp, G. A. and Liberzon, A. 2010 Long-Duration Time-Resolved PIV to study unsteady aerodynamics. *IEEE Transactions on Instrumentation and Measurement*. **59**, 3262-3269.

Taylor, Z. J., Gurka, R. and Kopp, G. A. 2014 Effects of leading edge geometry on the vortex shedding frequency of an elongated bluff body at high Reynolds number. *Journal of Wind Engineering and Industrial Aerodynamics*. **128**, 66-75.

Tieleman, H. W., Surry, D. and Mehta, K. C. 1996 Full/model scale comparison of surface pressures on the Texas Tech Experimental building. *Journal of Wind Engineering and Industrial Aerodynamics*. **61**, 1-23.

Tieleman, H. W. 2003 Wind tunnel simulation of wind loading on low-rise structures: a review. *Journal of Wind Engineering and Industrial Aerodynamics*. **91**, 1627-1649.

Wu, C-H. and Kopp, G. A. 2016 Estimation of wind-induced pressures on a low-rise building using quasi-steady theory. *Frontiers in Built Environment*. **2**, 00005.